Quantifying the Airflow Distortion over Merchant Ships. Part II: Application of the Model Results

BENGAMIN I. MOAT AND MARGARET J. YELLAND

National Oceanography Centre, Southampton, United Kingdom

ANTHONY F. MOLLAND

School of Engineering Sciences, Ship Science, University of Southampton, Southampton, United Kingdom

(Manuscript received 23 May 2005, in final form 29 August 2005)

ABSTRACT

Wind speed measurements obtained from ship-mounted anemometers are biased by the presence of the ship, which distorts the airflow to the anemometer. Previous studies have simulated the flow over detailed models of individual research ships in order to quantify the effect of flow distortion at well-exposed anemometers, usually sited on a mast in the ship's bows. In contrast, little work has been undertaken to examine the effects of flow distortion at anemometers sited on other merchant ships participating in the voluntary observing ship (VOS) project. Anemometers are usually sited on a mast above the bridge of VOS where the effects of flow distortion may be severe. The several thousand VOS vary a great deal in shape and size and it would be impractical to study each individual ship.

This study examines the airflow above the bridge of a typical, or generic, tanker/bulk carrier/general cargo ship using computational fluid dynamics models. The results show that the airflow separates at the upwind leading edge of the bridge and a region of severely decelerated flow exists close to the bridge top with a region of accelerated flow above. Large velocity gradients occur between the two regions.

The wind speed bias is highly dependent upon the anemometer location and varies from accelerations of 10% or more to decelerations of 100%. The wind speed bias at particular locations also varies with the relative wind direction, that is, the angle of the ship to the wind. Wind speed biases for various anemometer positions are given for bow-on and beam-on flows.

1. Introduction

Wind speed measurements obtained from ship-mounted anemometers are subject to a bias caused by the presence of the ship distorting the airflow to the instrument (Ching 1976; Kahma and Leppäranta 1981; Dobson 1981). Quantifying this bias is important in order to obtain the accurate wind speed measurements needed for ocean–atmosphere model forcing, coupled ocean–atmosphere model validation, satellite validation, and to quantify and predict possible changes in climate. Previous studies (Yelland et al. 1998, 2002; Dupuis et al. 2003; Popinet et al. 2004) used computational fluid dynamics (CFD) models to simulate the flow over detailed models of individual research ships in order to quantify the effect of flow distortion at anemometers usually sited in well-exposed positions, such as on a mast in the bow of the ship. In contrast, little work has been done to quantify the effect of flow distortion on wind speed reports obtained from anemometers mounted on voluntary observing ships (VOS). This is due to the large number of merchant ships (more than 6000) participating in the VOS program, the relatively large turnover of VOS (approximately 10% join/leave each year), and the large variation in ship type, size, and shape. Dobson (1981) suggested a simple approach based on predicting the vorticity above a simple box representation of a ship, but this was never employed since the required empirical constants were never measured.

This paper presents a method for predicting the wind speed bias for fixed anemometers above the bridge of tankers, bulk carriers, and general cargo ships using

Corresponding author address: Dr. B. I. Moat, National Oceanography Centre, European Way, Southampton SO14 3ZH, United Kingdom.
E-mail: bim@noc.soton.ac.uk

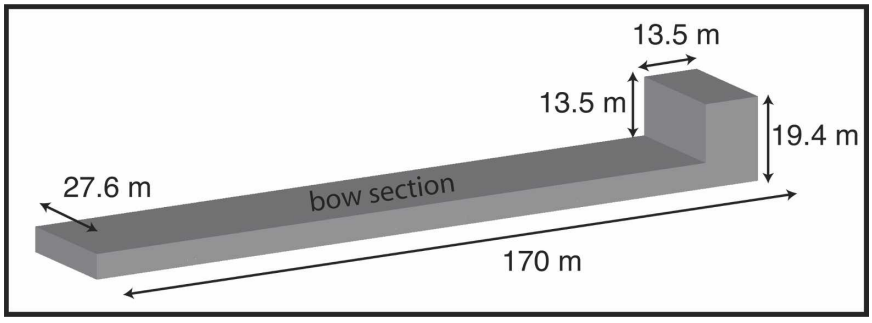

FIG. 1. The generic representation of a tanker/bulk carrier geometry.

numerical studies of the flow over the bow and beam of a generic, or typical, ship shape. Section 2 describes the formulation of the generic ship shape used to represent all three types of VOS. Section 3 gives a brief description of the CFD simulations of the airflow over the generic ship shape for both bow-on and beam-on wind directions. Section 4 presents a method to predict the wind speed bias for fixed anemometers above the bridge of the generic ship, and examines how the bias varies with anemometer position and with relative wind direction. Recommendations for locating anemometers on merchant ships are made and the possible effects of localized mast and spars on the mean flow are also discussed.

2. Generic ship models

Since 1995 information on the ship and type of instrumentation used by individual ships participating in the VOS program have been made available in the World Meteorological Organization (WMO) International List of Selected, Supplementary and Auxiliary Ships (known as Publication 47, hereafter WMO47). Originally, WMO47 was published annually (e.g., WMO 1994), but from 1998 it has been published quarterly. Between 1970 and 1995 the only information available on the anemometer location was the height of the instrument above the sea surface. In 1995 information on the ships length, breadth, freeboard, and type were included. Since 2002 the number of fields in WMO47 has been further increased to include the ship's draft, cargo height, and distance of the bridge from the bow. In addition, the location of the anemometer (e.g., mainmast, foremast, etc.), height of the anemometer above the deck, its distance from the bow, and its distance from the centerline are now also reported for each ship. With this recent increase in the ship and instrument metadata contained in WMO47 (Kent et al. 2006), predicting the wind speed bias at anemometer sites on VOS has become more realistic since the anemometer location and the ship type and dimensions are now known.

The VOS fleet can be roughly divided into a number of ship types such as 1) liquid tankers, 2) bulk carriers, 3) container ships, 4) gas tankers, 5) general cargo ships, and 6) others (e.g., ferries, research vessels, etc.). Moat et al. (2005) examined the principal dimensions of 71 individual ships and showed that the first three of these ship types can each be represented by a simple geometry since the principal ship dimensions (e.g., the height of the bridge above the deck, and the height of the bridge above the waterline) scale linearly with the ship's length. Kent et al. (2006) found similar results from a much larger sample of ships. Moat et al. (2005) also showed that tankers and bulk carriers could both be represented by one simple geometry (Fig. 1). Similarly, comparison of tankers and general cargo ship using metadata from WMO47 and the Lloyds of London Register of Ships shows that these types are also of very similar shape. This is illustrated in Fig. 2, which shows the height of the bridge above the deck for the two ship types. The linear relationship of Moat et al. (2005) is overlaid in the figure and discussed in section 4c. Provided no large deck-mounted cargo-handling systems are present, tankers, bulk carriers, and general cargo ships can thus be treated together as one ship type (hereafter referred to as a generic ship). Taken together these three types represent about 47% of the VOS fleet.

Container ships are not directly considered in the present study since Moat et al. (2005) showed that the large upwind obstacle presented by the containers significantly influenced the flow above the bridge. In addition, there is currently no information on the loading pattern of the containers and the effect of irregular loading on the pattern of the airflow above the bridge is not known. However, the results of this study can be applied to all ship types, including container ships, when the wind is blowing onto the beam of the ship (section 4a).

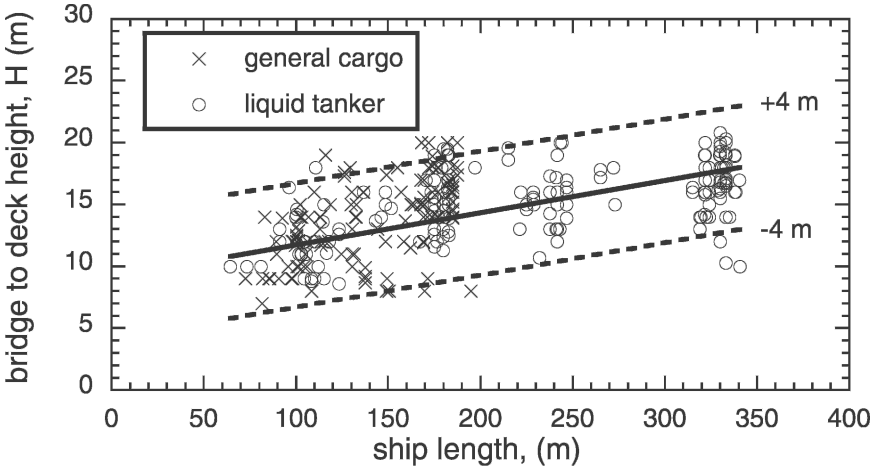

FIG. 2. Variation of the bridge to deck height, *H*, with ship length. The solid line indicates the linear fit [Eq. (1)] to the data of Moat et al. (2005).

3. The CFD simulations

The CFD simulations were performed using the commercially available code VECTIS (Ricardo 2001). Numerical simulations have advantages over performing physical wind tunnel or water channel tests. The whole flow field can be examined rather than measuring the airflow within small areas or single measurement locations and the simulations are easily repeatable. However, the computational mesh required to solve the flow field around complex geometries can be time consuming to generate. VECTIS generates the mesh in a fast, efficient manner and Moat et al. (2006, hereafter Part I) demonstrated that the code performed well in simulating the flow over bluff bodies. Part I showed that the VECTIS simulations of the flow speed above a surface-mounted block generally agreed to within 4% with wind speed measurements made above the bridge of a ship for a beam-on flow.

A simulation of a flow directly over the bow of a generic ship was performed. The principal dimensions of the generic ship were calculated using the method of Moat et al. (2005) and are contained in Fig. 1. The actual ship geometry used in this study was scaled down by 1:46, which was comparable in size to that of the model used in the VECTIS validation study performed in Part I. The simulation was run on an Origin 200 UNIX workstation, employed 630 000 computational cells, and took approximately 2 weeks to converge to a steady-state solution. A uniform wind speed profile of 7 m s^{-1} was specified at the inlet. Details of the code and methodology used are given in greater detail in Part I.

A beam-on flow was studied using a simulation of the flow directly over the beam of the ship with the bow section removed. The bow section has no effect on the flow above the bridge at this wind direction and its removal significantly reduced the time taken for the simulation to converge. The simulation was run at the High Power Computing facility at the National Oceanography Centre, Southampton, United Kingdom; used 600 000 cells; and converged to a steady-state solution within 5 days.

4. The mean airflow above the bridge

a. The general flow pattern

This section describes the results of the CFD simulations of the flow over (a) the bow of the generic ship geometry and (b) the surface-mounted block used to represent a beam-on flow over the bridge of a ship. An additional CFD simulation with no model geometry present was performed to determine the free-stream wind speed in the region of the ship's bridge. The results were normalized by this undisturbed, or free stream, wind speed.

The flow pattern above the bridge of the ship for bow-on flows has the same general characteristics as a flow over a surface-mounted cube (Hunt et al. 1978; Murakami et al. 1993). Figure 3 shows normalized wind speeds along the centerline above the bridge. There is flow separation at the leading edge of the bridge with deceleration of the airflow by up to 100% close to the bridge top where the flow is unsteady and reverses in direction. The height at which the wind speed equals the free-stream wind speed (i.e., a normalized wind speed of 1.0) varies from just above the upwind edge of the bridge and increases with distance downstream. Locating anemometers close to the vicinity of this line is

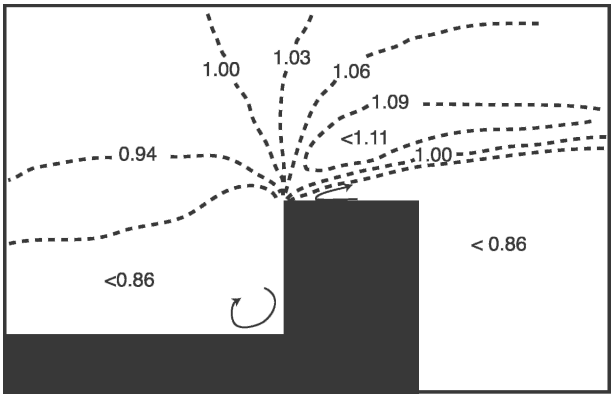

FIG. 3. The normalized wind speed along the centerline of the generic ship for a bow-on flow (from left to right). The contours indicate the normalized wind speed (i.e., the measured wind speed as a fraction of the free-stream wind speed). The arrows indicate regions of recirculation.

not recommended, as the velocity gradients are large. Above the line the airflow is accelerated by about 10% or more. The magnitude of the acceleration decreases with height.

Beam-on and bow-on flows are compared directly in Fig. 4, which shows a vertical profile of normalized wind speed from each simulation. To make a direct comparison, all distances have been normalized by the "step height," H. For the bow-on flow H is the height of the bridge above the ship's bow, and for a beam-on flow H is the height of the bridge above the waterline. The two profiles are obtained at a distance downwind of the leading edge, x/H, of 0.3 and both are on the centerline of the ship/block. The height above the bridge is given as z/H. The leading edge of the bridge is at $x = 0 = z$. Compared to the bow-on flow, the beam-on flow has a slightly thicker recirculation region and a stronger flow counter to the mean flow direction close to the bridge top.

The results for the bow-on and beam-on simulations are given in Tables 1 and 2, respectively, where the wind speed bias, expressed as a percentage of the free-stream flow speed, is shown on a vertical plane along the center of the bridge/block. Table 3 shows the difference between the two in the predicted acceleration of the flow for a given normalized position. The difference in the depth of the recirculation regions combined with the large velocity gradients in this area leads to large differences in the predicted wind speed for heights below about $z/H = 0.2$. The cause of the different depths is not known, but it is possible that, for bow-on flows, the flow above the bridge may be affected by the upwind distortion of the flow over the bow of the ship. For heights above $z/H = 0.2$ the two simulations agree very well, with bow-on and beam-on flows agreeing to within a few percent.

b. *Off centerline flows*

The results discussed above were all obtained along the centerline of the geometries. In contrast, Fig. 5 shows horizontal lines of the normalized wind speed across the bridge top at various heights. The lines are obtained at a distance downwind of the leading edge, x/H, of 0.3. As the sides of the bridge are approached, the normalized wind speed increases significantly within the decelerated region, at heights below $z/H = 0.2$. This is the result of the flow being affected by the

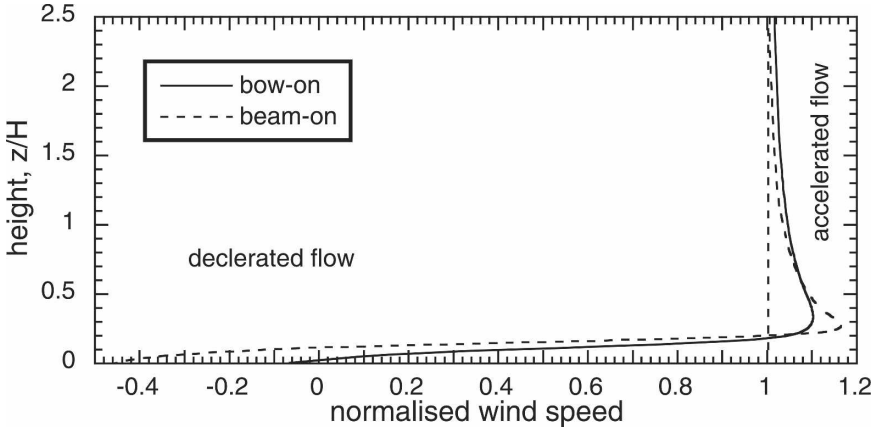

FIG. 4. Vertical profiles of normalized wind speed at a distance of $x/H = 0.3$ from the upwind leading edge (located at $x = 0 = z$). The heights have been normalized by the step height, H. For beam-on flows, H is the bridge-to-waterline height and for bow-on flows H is the bridge-to-deck height. A negative normalized wind speed indicates flow reversal. The vertical dashed line indicates the region where the wind speed is equal to the free-stream wind speed.

TABLE 1. Predicted wind speed bias for anemometers located on the centerline of the ship for flows directly over the bow. The bias is expressed as a percentage of the free-stream wind speed. A negative bias indicates a decelerated flow and values in boldface indicate the flow is counter to the main flow. All distances have been scaled by the bridge-to-deck height, H. The values set in italics represent the estimated anemometer position in the example discussed in section 4d.

Height,	Distance from front edge of bridge, x/H								
z/H	0.0	0.1	0.2	0.3	0.4	0.5	0.6	0.7	0.8
0.003	−20	**−76**	**−93**	**−94**	**−91**	**−89**	**−87**	**−86**	**−86**
0.1	4	−5	−34	−58	−72	−80	−85	−89	−93
0.2	3	8	8	4	−4	−15	−27	−38	−47
0.3	4	7	9	10	10	9	7	4	0
0.4	4	6	9	10	11	*11*	11	10	9
0.5	4	5	7	9	10	*11*	11	11	11
0.6	3	5	6	8	*9*	*10*	*10*	*10*	10
0.7	3	4	6	7	8	*8*	9	9	9
0.8	3	4	5	6	7	*7*	8	8	8
0.9	3	4	4	5	6	6	7	7	7
1.0	3	3	4	5	5	6	6	7	7
1.2	2	3	3	4	4	5	5	5	5
1.6	2	2	2	3	3	3	4	4	4
2.0	2	2	2	2	2	3	3	3	3
2.4	1	1	2	2	2	2	2	2	2

upwind corner of the bridge and the airflow deflecting around the side of the ship. However, above a height of $z/H = 0.3$ the normalized wind speeds do not vary by more than 2% across the width of the bridge. This suggests that the results shown in Tables 1 and 2 can be applied to all anemometers positions, regardless of their cross-flow position, as long as they are not sited within the decelerated region on a cross-flow edge. For example, the upwind corner would affect wind speed measurements obtained from an anemometer on a short mast located on the forward edge of the bridge for beam-on flows.

c. Predicting the wind speed bias above the bridge

The results in Tables 1 and 2 can be used to quantify the wind speed bias if the anemometer position and the relevant step height, H, are known for a particular ship. This information has been available in WMO47 since 2002. Wind speed biases can be determined for VOS anemometer wind speed reports prior to 2002 using either (a) the WMO47 metadata if the ship is still submitting reports after 2002 or (b) the ship dimensions estimated by the method of Moat et al. (2005), as described below. In the second case an assumption of the anemometer position will have to be made.

For any individual ship the step height, H, differs with relative wind directions. For bow-on flows H is the height of the bridge top above the deck and for beam-on flows H is the height of the bridge top above the waterline. The bridge-to-deck height and waterline heights can be calculated from the ships overall length (LOA) using the relationships given in Table 1 of Moat et al. (2005). LOA can be obtained from Lloyds of London Register of Ships. For bow-on flows

$$H = 9.11 + 0.026 \times \text{LOA}, \quad (1)$$

and similarly for beam-on flows

$$H = 10.65 + 0.0515 \times \text{LOA}. \quad (2)$$

The equations were derived from the dimensions of 44 ships (RINA 1990–1993) examined by Moat et al. (2005). These relationships are very similar to those

TABLE 2. As in Table 1, but for beam-on flows. All distances have been scaled by the bridge-to-waterline height, H.

Height,	Distance from front edge of bridge, x/H												
z/H	0.0	0.1	0.2	0.3	0.4	0.5	0.6	0.7	0.8	0.9	1.0	1.2	1.4
0.002	−2	**−63**	**−55**	**−54**	**−60**	**−69**	**−79**	**−88**	**−96**	−97	−90	−79	−70
0.1	13	−17	−86	**−89**	**−87**	**−93**	**−99**	−93	−86	−80	−73	−62	−54
0.2	9	17	16	1	−24	−40	−46	−47	−48	−46	−44	−38	−34
0.3	7	12	15	16	15	12	7	3	*−2*	−4	−7	−9	−10
0.4	6	9	11	12	12	12	*11*	*10*	*9*	*8*	7	6	4
0.5	4	7	8	10	10	10	10	9	*9*	8	8	6	6
0.6	4	5	7	7	8	8	8	8	8	7	7	6	5
0.7	3	4	5	6	7	7	7	7	7	6	6	5	5
0.8	3	4	4	5	6	6	6	6	6	6	6	5	5
0.9	2	3	4	4	5	5	5	5	5	5	5	5	4
1.0	2	3	3	4	4	4	4	4	5	4	4	4	4
1.2	2	2	2	2	3	3	3	3	3	3	3	3	3
1.6	1	1	1	2	2	2	2	2	2	2	2	2	2
2.0	1	1	1	1	1	1	1	1	1	1	1	1	1
2.4	0	0	0	1	1	1	1	1	1	1	1	1	1

TABLE 3. Difference between Tables 1 and 2, i.e., bow-beam bias for given scaled positions.

Height,	Distance from front edge of bridge, x/H								
z/H	0.0	0.1	0.2	0.3	0.4	0.5	0.6	0.7	0.8
~0	−18	−13	−38	−40	−31	−20	−8	2	10
0.1	−9	12	52	31	15	13	14	4	−7
0.2	−6	−9	−8	3	20	25	19	9	1
0.3	−3	−5	−6	−6	−5	−3	0	1	2
0.4	−2	−3	−2	−2	−1	−1	0	0	0
0.5	0	−2	−1	−1	0	1	1	2	2
0.6	−1	0	−1	1	1	2	2	2	2
0.7	0	0	1	1	1	1	2	2	2
0.8	0	0	1	1	1	1	2	2	2
0.9	1	1	0	1	1	1	2	2	2
1.0	1	0	1	1	1	2	2	3	2
1.2	0	1	1	2	1	2	2	2	2
1.6	1	1	1	1	1	1	2	2	2
2.0	1	1	1	1	1	2	2	2	2
2.4	1	1	2	1	1	1	1	1	1

found more recently by Kent et al. (2006) using a much larger sample of ships. Figure 2 shows that the bridge-top-to-deck height increases linearly with ship length. The bridge is located above an accommodation block, which is made up of four, five, or six decks depending upon ship length. Over the full range of ship lengths, from 70 to 330 m, there are variations of ±4 m in the bridge-to-deck height. For the dataset, 84% of the data are contained within this range.

Kent and Taylor (1991) gave descriptions of a small number of VOS, along with details of instrument types and locations. The ships that carried fixed anemometers generally did so on a mast above the bridge, located on the ship's centerline. The masts were usually well aft of the forward edge of the bridge and carried the anemometers at heights of 6–10 m above the top of the bridge. Similarly, Kent et al. (2006) found average anemometer heights above the deck of about 9 m for tankers and bulk carriers. Of the available metadata for VOS reporting in the second quarter of 2004, over 80% of anemometers were located within 3 m of the centerline of the ship (E. C. Kent 2005, personal communication).

d. Sensitivity of the model results to uncertainties in H and anemometer positions

In the following example a ship of 200-m length will be used to examine the sensitivity of the model results to uncertainties in the estimated anemometer location and ship dimensions, and the results are indicated by the values set in italics in Tables 1 and 2. The ship's breadth, B, and bridge length, L, can be calculated from the ship's LOA using the relationships given in Table 1 of Moat et al. (2005), which are reproduced here:

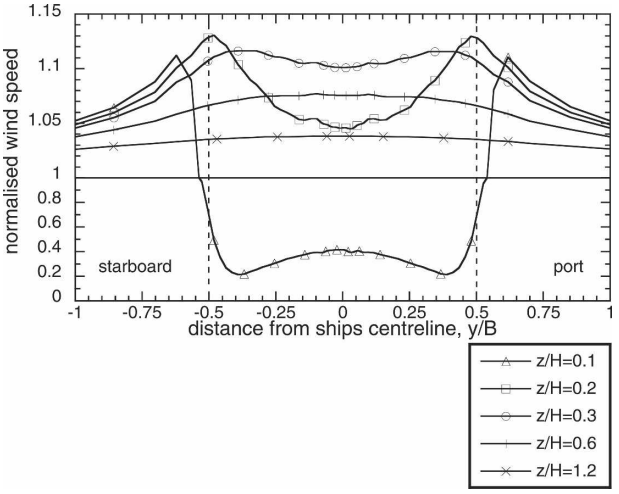

FIG. 5. Normalized wind speed profiles across the bridge top at distances of $x/H = 0.3$ downwind of the front edge of the bridge for bow-on flows. Every fifth data point is shown and the horizontal scale is normalized by the ship's breadth, B. The dashed vertical lines indicate the port and starboard edges of the ship's bridge. Note change of scale at 1.0 on the vertical axis.

$$B = -3.00 + 0.18 \times \mathrm{LOA} \quad \text{and} \tag{3}$$

$$L = 10.16 + 0.0198 \times \mathrm{LOA}. \tag{4}$$

These relationships suggest a bridge length of 14 m and a width of 33 m, and Eqs. (1) and (2) suggest a bridge-to-deck height of 14 m and a bridge-to-waterline height of 21 m. The mast is assumed to lie on the centerline of the ship, halfway between the forward and aft edges of the bridge top (i.e., distance downwind of the leading edge, x, is 7 m for bow-on flow and about 16 m for beam-on flow). The anemometer will be assumed to be at a height z of 8 m above the bridge top.

For bow-on flows H could vary from about 10 to 18 m, which would lead to a scaled anemometer height in the range $0.4 < z/H < 0.8$. Hence, for bow-on flows the uncertainty in H produces only a few percent uncertainty in the predicted flow speed regardless of the distance, x, of the anemometer downwind of the leading edge (Table 1). Varying the anemometer height, z, by 2 m has a similar impact.

For beam-on flows H could range from about 17 to 25 m, which would lead to a scaled anemometer height in the range $0.3 < z/H < 0.5$. Our assumed anemometer position ($0.6 < x/H < 0.9$) is thus near the top of the region of decelerated flow where the velocity gradients are very large and the modeled results (Table 2) would suggest wind speed biases of the order of −2% to 11%. Again, varying the anemometer height, z, by 2 m has a similar impact. For beam-on flows it can be seen that the predicted bias may be sensitive to the exact value of

all the estimated parameters (H, anemometer position and anemometer height), as anemometers may be located close to, or within, the decelerated region where the velocity gradients are high. This sensitivity will decrease with decreasing ship length since the height of the anemometer above the top of the bridge is relatively independent of ship length; that is, the scaled anemometer height is larger for smaller ships.

e. Other wind directions

For relative wind directions other than beam-on or bow-on, the distance of the anemometer from the upwind leading edge varies with the angle θ of the wind from the perpendicular with the geometry as

$$x = \frac{x_0}{\cos\theta}, \tag{5}$$

where x_0 is the distance of the anemometer from the upwind leading edge for bow-on flows. In the example given in section 4d for beam-on flows, $x/H = 0.76$ for $\theta = 0°$ and $x/H = 0.88$ for $\theta = 30°$.

As the relative wind direction moves from the bow toward the beam, the value of the step height, H, will change from the bridge-to-deck height to the bridge-to-sea level height. Moat et al. (2004) used wind tunnel studies to examine the flow over a block and showed that there was no significant variation in normalized wind speed with a change in relative wind direction of $\pm 30°$. It is therefore thought that the predicted wind speed biases given in Tables 1 and 2 can be applied for relative wind directions within 30° of the bow and beam, respectively, as long as the change in x is taken into account.

f. Applicability of the results

The results in Table 1 are applicable for tankers, bulk carriers, and general cargo ships for flows within 30° of bow-on as long as the ship does not carry large deck-mounted cranes or other significant upwind obstacles. The results in Table 2 can be applied to all ship types, rather than just tankers, bulk carriers, and general cargo ships, since almost all ships present a single-stepped obstacle to flows within 30° of beam-on. The only exception to this is if the mast is located at the forward (bow-most) edge of the bridge, that is, at the cross-wise edge for a beam-on flow (section 4b, Fig. 5).

This method does not take into account the flow distortion caused by small-scale objects such as masts and spars. The work of Dabberdt (1968a, 1968b) and Cermak and Horn (1968) has shown that anemometers located within two mast diameters of lattice masts and spars may measure flows that have been accelerated by up to 20% or decelerated by 40%, depending on the relative wind direction. To achieve wind speed measurements that are accurate to within 5% of the undisturbed wind speed, Gill et al. (1967) recommends that anemometers should be located not less than three mast diameters from solid cylindrical masts. These previous studies did not take into account the effect of supporting platforms typically found on ships. The simulation of the airflow directly over the bow of the RRS *Charles Darwin* (Yelland et al. 1998) was repeated with the foremast removed in order to separate the effects of the large-scale obstruction due to the ship's superstructure from those due to small-scale obstruction of the foremast. A comparison of the two simulations showed that the flow distortion at four anemometer locations on the foremast (Fig. 6) was not only dependent on the location of the anemometer to the cylindrical foremast extension but also the platform itself. The results of both simulations are detailed in Table 4 and show that anemometers located closer to the foremast extension (diameter of 0.2 m) were affected to a greater extent (4%) than those at a greater distance (<1%), which supports the findings discussed above. The Kaijo-Denki anemometer, located in front of the foremast platform, was affected to a greater extent (9%) than those located directly above the platform (<4%). Therefore, anemometers should be located as far as possible abeam of the mast and as high as possible above, rather than in front of, the measuring platform.

Metadata are becoming available (see Kent et al. 2006) that provide information as to the position of the anemometer relative to the ship's centerline, that is, a distance to port, or to starboard, so it will be possible to determine whether the anemometer was downwind of the mast (assuming the mast lies on the centerline). Unfortunately, no other data are available about the size of the mast or other local obstructions.

The results in Table 2 could also be applied to ships that carry instruments on a mast in the bows rather than above the bridge provided that the accommodation block (or any other large obstacle such as container stacks) is located at a sufficient distance aft of the anemometer. The flow distortion in front of the block is shown in Fig. 7 and it is apparent that to reduce the flow distortion to less than 6% of the free-stream wind speed an anemometer must be located at a distance of over twice the obstacle height upwind. The CFD results for the no-foremast model of the RRS *Charles Darwin* show that the ship's superstructure causes a 3%–5% deceleration of the flow at the four anemometer sites (overlaid in Fig. 7), in good agreement with the results from the block model.

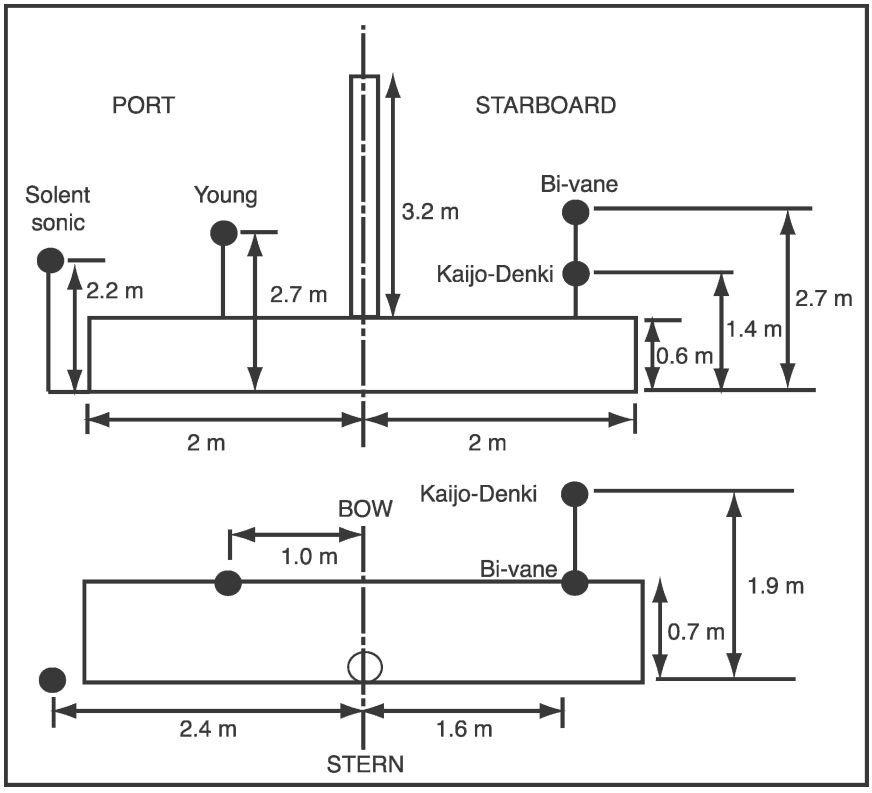

FIG. 6. Positions of the anemometers on the foremast platform of the RRS *Charles Darwin* looking from (top) astern and (bottom) above.

g. Recommendations for locating anemometers

It is clear from the results discussed above that anemometers should be located as high as possible in order to minimize the effects of flow distortion and to avoid the anemometer being located in the decelerated flow region for beam-on winds. The area where the normalized wind speed equals 1.0 should also be avoided, as the velocity gradients and the uncertainty in the wind speed bias are both large. Mounting anemometers toward the forward edge of the bridge top also reduces the effects of flow distortion, but a position directly above the forward edge is not recommended since the results for beam-on flows in Table 2 do not apply in that area (section 4b) if the anemometer is located within, or close to, the decelerated region.

If anemometers are located above platforms or walkways, they should be positioned as high as possible above the platform rather than in front of it. Anemometers located above yardarms should be located over three yardarm diameters above the yard.

5. Summary

CFD simulations of the airflow over a generic representation of tankers, bulk carriers, and general cargo ships have been made for bow-on and beam-on flows. If

TABLE 4. Wind speed errors Δu at anemometer sites on the RRS *Charles Darwin* as calculated from CFD models. The with-foremast results of Yelland et al. (1998) are compared to a later simulation with the foremast platform removed. The difference between the two represents the effect of the platform itself.

Anemometer	Height above platform (m)	Distance from foremast extension (mast diameters)	With foremast Δu (%)	No foremast Δu (%)	Difference
Solent sonic	2.2	12	−3.5	−3.0	0.5
RM Young	2.6	5	−9.0	−5.0	4.0
Bi-vane	2.7	8	−6.0	−4.0	2.0
Kaijo-Denki	1.4	8	−13.5	−4.5	9.0

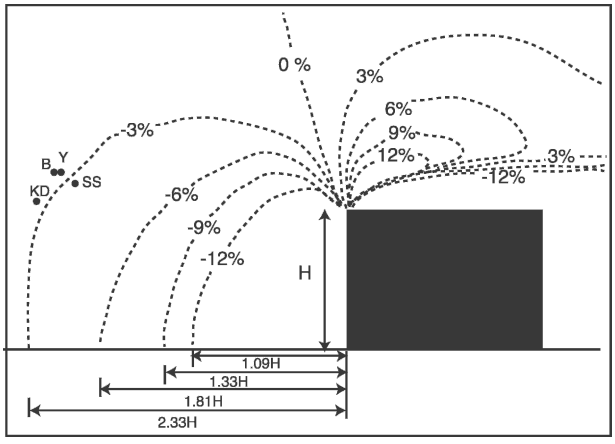

FIG. 7. The flow distortion in front of the block for a beam-on flow. The contours show the wind speed as a percentage of the free-stream, or undisturbed, wind speed. The symbols correspond to the relative positions of the Solent Sonic (SS), RM Young (Y), Bi-vane, and the Kajio-Denki (KD) anemometers located on the RRS *Charles Darwin*. The flow direction is from left to right.

a ship's dimensions and anemometer position are included in the WMO47 metadata, then the bias in the mean wind speed measurement can be directly determined using the results in (a) Table 1 for flows within 30° of bow-on over tankers, bulk carriers, and general cargo ships, and (b) Table 2 for flows within 30° of beam-on for all ships. If the metadata are not available, an estimate of the ship dimensions can be made using the method suggested by Moat et al. (2005) using (a) ship type and length obtained from the Lloyds of London Register of Ships, and (b) some assumptions with regard to typical anemometer positions. The latter assumptions may be verified once a suitable range of metadata is available from WMO47.

The results showed that the wind speed bias depends on the height of the anemometer and on its position downwind of the leading edge of the bridge. However, the results are independent of the anemometer's position relative to the cross-wind edge of the bridge, as long as it is not placed below a height of $z/H = 0.2$ directly above that edge. For a given anemometer position the bias also varies with the direction of the ship to the wind since (a) the step height varies from the bridge-to-deck height for bow-on flows to bridge-to-waterline height for beam-on flows, and (b) the distance, x, of the anemometer downwind of the leading edge varies with relative wind direction. The mean wind speed bias varies from 100% deceleration in the recirculation region directly above the bridge to 10% or more in the accelerated area above the recirculation region. To minimize the effects of flow distortion, anemometers should be mounted (a) as high as possible above the bridge top and (b) toward, but not at, the forward edge of the bridge top. The anemometer should be located at a distance greater than three mast diameters from the supporting mast and be located above the platform rather than in front of it.

Acknowledgments. The authors wish to thank Dr. Peter K. Taylor (National Oceanography Centre, United Kingdom) and Mr. Val Swail (Meteorological Service of Canada) for their support and encouragement, and Dr. Elizabeth Kent (National Oceanography Centre, United Kingdom) for sharing her considerable knowledge of VOS characteristics. This project was partially funded by the Meteorological Service of Canada and the Woods Hole Oceanographic Institution.

REFERENCES

Cermak, J. E., and J. D. Horn, 1968: Tower shadow effect. *J. Geophys. Res.,* **73,** 1869–1876.

Ching, J. K. S., 1976: Ship's influence on wind measurements determined from BOMEX mast and boom data. *J. Appl. Meteor.,* **15,** 102–106.

Dabberdt, W. F., 1968a: Tower induced errors in wind profile measurements. *J. Appl. Meteor.,* **7,** 359–366.

——, 1968b: Wind disturbance by a vertical cylinder in the atmospheric boundary layer. *J. Appl. Meteor.,* **7,** 367–371.

Dobson, F. W., 1981: Review of reference height for and averaging time of surface wind measurements at sea. Marine Meteorology and Related Oceanographic Activities Rep. 3, WMO, Geneva, Switzerland, 64 pp. [Available from World Meteorological Organization, Case Postale 5, CH-1211 Geneva 20, Switzerland.]

Dupuis, H., C. Guerin, D. Hauser, A. Weill, P. Nacass, W. M. Drennan, S. Cloche, and H. C. Graber, 2003: Impact of flow distortion corrections on turbulent fluxes estimated by the inertial dissipation method during the FETCH experiment on R/V *L'Atalante*. *J. Geophys. Res.,* **108,** 8064, doi:10.1029/2001JC001075.

Gill, G. C., L. E. Olsson, J. S. Sela, and M. Suda, 1967: Accuracy of wind measurements on towers and stacks. *Bull. Amer. Meteor. Soc.,* **48,** 665–674.

Hunt, J. C. R., C. J. Abell, J. A. Peterka, and H. Woo, 1978: Kinematical studies of the flows around free or surface-mounted obstacles; applying topology to flow visualisation. *J. Fluid Mech.,* **86,** 179–200.

Kahma, K. K., and M. Leppäranta, 1981: On errors in wind speed observations on R/V *Aranda*. *Geophysica,* **17,** 155–165.

Kent, E. C., and P. K. Taylor, 1991: Ships observing marine climate: A catalogue of the voluntary observing ships participating in the VOSP-NA. Marine Meteorology and Related Oceanographic Activities Rep. 25, World Meteorological Organization, 123 pp.

Moat, B. I., A. F. Molland, and M. J. Yelland, 2004: A wind tunnel study of the mean airflow around a simple representation of a merchant ship. SOC Research and Consultancy Rep. 87, Southampton Oceanography Centre, Southampton, United

Kingdom, 21 pp. [Available from National Oceanography Centre, European Way, Southampton SO14 3ZH, United Kingdom.]

——, M. J. Yelland, R. W. Pascal, and A. F. Molland, 2005: An overview of the airflow distortion at anemometer sites on ships. *Int. J. Climatol.,* **25,** 997–1006.

——, ——, ——, and ——, 2006: Quantifying the airflow distortion on merchant ships. Part I: Validation of a CFD model. *J. Atmos. Oceanic Technol.,* **23,** 341–350.

Murakami, S., A. Mochida, and Y. Hayashi, 1993: Comparison of various turbulence models applied to a bluff body. *J. Wind Eng. Indust. Aerodyn.*, **46/47,** 21–36.

Popinet, S., M. Smith, and C. Stevens, 2004: Experimental and numerical study of the turbulence characteristics of airflow around a research vessel. *J. Atmos. Oceanic Technol.,* **21,** 1575–1589.

Ricardo, 2001: VECTIS computational fluid dynamics (release 3.5). Ricardo Consulting Engineers Ltd., Shoreham-by-Sea, United Kingdom, 262 pp. [Available from Ricardo Consulting Engineers Ltd., Bridge Works, Shoreham-by-Sea, West Sussex BN43 5FG, United Kingdom.]

RINA, 1990–1993: Significant ships. The Royal Institution of Naval Architects, London, United Kingdom.

WMO, 1994: International list of selected, supplementary and auxiliary ships. WMO Rep. 47, Geneva, Switzerland.

Yelland, M. J., B. I. Moat, P. K. Taylor, R. W. Pascal, J. Hutchings, and V. C. Cornell, 1998: Wind stress measurements from the open ocean corrected for airflow distortion by the ship. *J. Phys. Oceanogr.,* **28,** 1511–1526.

——, ——, R. W. Pascal, and D. I. Berry, 2002: CFD model estimates of the airflow over research ships and the impact on momentum flux measurements. *J. Atmos. Oceanic Technol.,* **19,** 1477–1499.